Quantum Chemistry Study on the Structures and Electronic Properties of Bimetallic Ca₂-Doped Magnesium Ca₂Mg$_n$ (n = 1–15) Clusters

Chenggang Li [1,2], Yingqi Cui [1,*], Hao Tian [1], Baozeng Ren [2], Qingyang Li [3], Yuanyuan Li [3] and Hang Yang [3]

[1] Quantum Materials Research Center, College of Physics and Electronic Engineering, Zhengzhou Normal University, Zhengzhou 450044, China; zznu_lcg@163.com (C.L.); zznu_lf@163.com (H.T.)
[2] School of Chemical Engineering and Energy, Zhengzhou University, Zhengzhou 450001, China; zznurbz@163.com
[3] School of Physics and Electronic Engineering, Sichuan University of Science & Engineering, Zigong 643000, China; zznmuszg@163.com (Q.L.); zznucyq@163.com (Y.L.); zznutyn@163.com (H.Y.)
* Correspondence: zznu_llm@163.com

Abstract: Here, by utilizing crystal structure analysis through the particle swarm optimization (CALYPSO) structural searching method with density functional theory (DFT), we investigate the systemic structures and electronic properties of Ca₂Mg$_n$ (n = 1–15) clusters. Structural searches found that two Ca atoms prefer to occupy the external position of magnesium-doped systems at n = 2–14. Afterward, one Ca atom begins to move from the surface into the internal of the caged skeleton at n = 15. Calculations of the average binding energy, second-order difference of energies, and HOMO–LUMO gaps indicated that the pagoda construction Ca₂Mg₈ (as the magic cluster) has higher stability. In addition, the simulated IR and Raman spectra can provide theoretical guidance for future experimental and theoretical investigation. Last, further electronic properties were determined, including the charge transfer, density of states (DOS) and bonding characteristics. We hope that our work will provide theoretical and experimental guidance for developing magnesium-based nanomaterials in the future.

Keywords: CALYPSO; DFT; stability; Ca₂Mg$_n$ clusters

1. Introduction

Nanomaterials with small particle sizes, specific surface areas and high surface energies possess wide applications in chemistry, physics, biology, medicine, materials and nanodevices. Magnesium atoms contain s^2 closed-shell electron configuration similarly to helium, which plays an essential role in aerospace, mobile electronics, automobile and biomedical applications [1–4]. Currently, metal-doped magnesium clusters with unique geometries and fascinating electronic properties have received considerable attention in magnesium-based multi-function materials.

In the past decades, many experimental techniques and theoretical studies have been reported for the related structures and properties of pure magnesium clusters [5–19]. For instance, on the experimental side, the transition points of Mg$_n$ clusters were determined at n = 20 by Diederich's group [5]. By measuring the photoelectron spectra and observing the sp band gaps of Mg$_n$ (n = 3–35) clusters, Thomas et al. found that the anion magnesium clusters exhibited a metallic character from n = 18 [6]. On the theoretical side, the ground state van der Waals potential of a magnesium dimer was described by five essential parameters of the Tang–Toennies potential model [7].

Janecek et al. studied the structures of neutral and cationic Mg$_n$ (n to 30) clusters using the local spin density functional [8]. Based on the MP4 (SDTQ) and CCSD(T) levels, the electron affinities were calculated for magnesium dimers and trimers [9]. By using the spin-unrestricted density functional theory with a local density approximation, Gong

and co-workers studied the electronic structures of Mg_n (n < 57) clusters [10]. Their results found that more $3p$ electrons will be involved in the sp hybridization with the cluster size increasing. More recently, Akola and co-workers focused on the structural and electronic properties of Mg_n (n < 13) clusters [11]. Their investigations showed that the onset of metallization of Mg_n clusters is difficult to assign due to the energy gap and sp hybridization.

Subsequently, electron binding energies, structural and electronic properties and the nonmetal-to-metal transition were studied systemically by Jellinek and Acioli [12,13]. In addition, by using ab initio theoretical methods (B3PW91, B3LYP and MP4), Lyalin et al. investigated the structure and electronic properties of neutral and singly charged Mg_n (n = 2–21) clusters [14]. The above study by Lyalin et al. suggested that the hexagonal ring structure determines the cluster growth from Mg_{15}. Moreover, the electronic shell effects and the Jellium-like behavior manifest themselves in the formation of geometrical properties; however, the shell effects do not determine the geometry of the Mg clusters completely.

In addition, the energetic structural properties of neutral magnesium clusters Mg_n (n = 2–22) were investigated utilizing density functional theory [15]. More recently, Heidari and Xia's groups presented further details about the structural transition and electronic properties of Mg_n (n = 10–56) and $Mg_n^{0/-}$ (n = 3–20) clusters, respectively [16,17]. Recently, Duanmu's group investigated the geometries, binding energies, adiabatic ionization potentials and adiabatic electron affinities of $Mg_n^{+/0/-}$ (n = 1–7) clusters [18] and cohesive energies by using the CCSD(T) scheme with MP2/CBS correction for Mg_n (n = 2–19 and 28), respectively [19].

Most recently, research found that heteroatom doping is an effective strategy to stabilize geometrical structures or to tune electronic properties. Up to now, based on the different quantum chemistry calculations, studies on metal-doped (Be, Al, Ge, Sn, $3d$ and $4d$ TM atoms) and nonmetal-doped (B, C, N, O, F and Si) magnesium clusters have harvested many great achievements [20–32]. More importantly, based on the CALYPSO structural searching method and DFT, the structures and electronic properties of Be-, Be_2-, Sr_2- and Ba_2-atom-doped differently sized magnesium clusters have been systemically discussed by Zeng's, Zhao's and our groups [33–37]. For example, Zeng and co-workers found that $BeMg_9^0$, $BeMg_9^{+1}$ and $BeMg_8^{-1}$ clusters possess relative highly stability out of the studied systems [33].

Moreover, the stability mainly originating from the σ-type covalent bond, is formed by the interaction between Be-s and Mg-p orbitals. Zhao's group performed the structural and electronic properties of $BeMg_n$ (n = 10–20) clusters and their anions [34]. The research concluded that the position of Be atom changes from completely encapsulated sites to surface sites after reverting to the caged magnesium motif. Subsequently, the structures and electronic properties have been investigated for two Be-, Sr- and Ba-atom-doped small-sized magnesium clusters by our group [35–37]. For Be_2Mg_n (n = 1–20) clusters, from n = 10, the structures transfer from $3D$ to filled cage-like frameworks [35].

Furthermore, in the small size, one Be atom prefers the surface sites, and the other Be atom tends to embed inside magnesium motif. However, for the large size clusters (n > 18), two Be atoms were completely encapsulated into magnesium cages. In addition, the Be_2Mg_8 cluster possesses robust stability, and Be-$2p$ and Mg-$3p$ orbitals revealed increasing metallic behavior. More interestingly, based on the same calculated method, studies on the structural evolution and electronic properties were performed for $SrMg_n^{0/-}$ (n = 1–12) clusters [36]. As a result, the tower-like framework of the Sr_2Mg_8 cluster possesses higher stability out of the studied systems.

Moreover, the stronger sp hybridization leads to stronger Sr-Mg bonds, which is supported by the analysis of the multi-center bonds. Subsequently, our groups systemically reported the structures and electronic properties of two-barium-atom-doped magnesium in both neutral and anionic species [37]. A pagoda-like Ba_2Mg_8 was determined by analyzing the relative stability.

Analysis of the molecular orbitals indicated that the high stability comes mainly from the interaction between Ba-6s and Mg-3p orbitals. In conclusion, the stronger sp hybridization leads to stronger M-Mg bonds and metallic behavior. Last, the geometric structures and electronic properties have been investigated systemically for lithium-doped magnesium clusters [38]. The results indicated that lithium atoms prefer to occupy the convex sites of LiMg$_n$ structures. The LiMg$_9$ cluster possesses relatively higher stability. In addition, the charges transfer from the Li to Mg atoms, and there exists strong hybridization among sp orbitals.

Thus, metal-atom-doped magnesium clusters provide an effective approach to creating novel structures and electronic properties. As the same group of alkaline earth metals, Ca and Be, Mg, Sr and Ba have the identical valence electronic configuration of ns^2. Nevertheless, due to the different electronegativity and atomic radius of Ca atoms compared with Be, Mg, Sr and Ba atoms, are there similar frameworks for two-calcium-atom-doped magnesium clusters? If yes, do these clusters possess novel electronic and bonding properties? How does hybridization change?

To date, minor investigations on the structures and electronic properties of two-calcium-atom-doped magnesium clusters have been reported in theoretical calculations and experimental works. Thus, in the present work, motivated by Be-, Mg-, Sr- and Ba-doped magnesium, we performed a systematic investigation for two-calcium-atom-doped magnesium Ca$_2$Mg$_n$ (n = 1–15) clusters.

First, we conducted wide structural searching and precise structural optimization to explore the structural evolution rule. Second, determining the stable configuration of Ca$_2$Mg$_n$ (n = 1–15) clusters was conducted by analyzing the stability properties. Finally, some electronic properties, such as the charge transfer, IR and Raman spectra, DOS and bonding characteristics, are discussed for Mg-doped alkaline-earth clusters. We hope that our investigations will provide a theoretical and experimental basis for studying the microscopic mechanism of magnesium doped with alkaline-earth nanomaterials.

2. Computational Detail

In the present section, a stochastic global search algorithm based on the CALYPSO structural searching method was used to obtain the lowest and low-lying isomers of Ca$_2$Mg$_n$ (n = 1–15) clusters and Mg$_{n+2}$ (n = 1–15) clusters [39–41]. Based on this method, the corresponding stable or metastable structures can be successful with the chemical composition and given external conditions [42–50], and the detailed searching process can be found in our reported papers [42–47]. The structural optimization and energy calculations employed the B3PW91 functional and 6$-$311+G(d) basis set for Ca and Mg atoms, respectively [51,52].

In particular, the B3PW91 functional has been widely tested for magnesium and magnesium-based clusters [35,36]. In addition, the spin multiplicity (1, 3, 5 and 7) is included, no imaginary frequencies are validated. All calculations were performed using the Gaussian09 program package [53]. In the following works, the relative stabilities of the ground state Ca$_2$Mg$_n$ (n = 1–15) and Mg$_{n+2}$ (n = 1–15) clusters were studied by computing the average binding energy (E_b) and second-order difference energy ($\Delta_2 E$). Subsequently, the IR and Raman spectra, DOS, molecular orbitals and AdNDP were systemically investigated using the Multiwfn software for the studied clusters [54]. To ensure the reliability of our computational method, the bond length (r_e), vibration frequencies (ω_e) and dissociation energies (D_e) were calculated for Mg$_2$, Ca$_2$ and CaMg dimers, respectively.

For the Mg$_2$ dimer, our calculated values were r_e = 3.651 Å, D_e = 0.0790 eV, which are in good agreement with the experimental results (3.891 Å, 0.0866 eV) [55]. For the Ca$_2$ and CaMg dimers, there are no experimental values available. Our calculated results for the bond lengths, vibration frequencies and dissociation energies are 4.2667 Å, 72.32 cm^{-1} and 0.1478 V for the Ca$_2$ dimer and 3.909 Å, 82.63 cm^{-1} and 0.1114 V for the CaMg dimer, respectively. Moreover, the bond length and frequency of Ca$_2$ dimer are also in excellent

agree with Soltani's theoretical values (4.285 Å and 65.2 cm^{-1}), respectively [56]. This indicated the reliability of the proposed method in this work.

3. Results and Discussions

3.1. Geometric Structures

In Figure 1, the lowest and lower-lying energy structures are present for Ca$_2$Mg$_n$ (n = 1–15) and Mg$_{n+2}$ (n = 1–15) clusters. These isomers with energies from low to high are designated by *na*, *nb*, *nc* and *nd*. Moreover, the electronic states and point symmetry are also collected in Table 1. Simultaneously, the Cartesian coordinates of the lowest energy structures of Ca$_2$Mg$_n$ (n = 1–15) clusters are given in Table S1 in the Supplementary Materials.
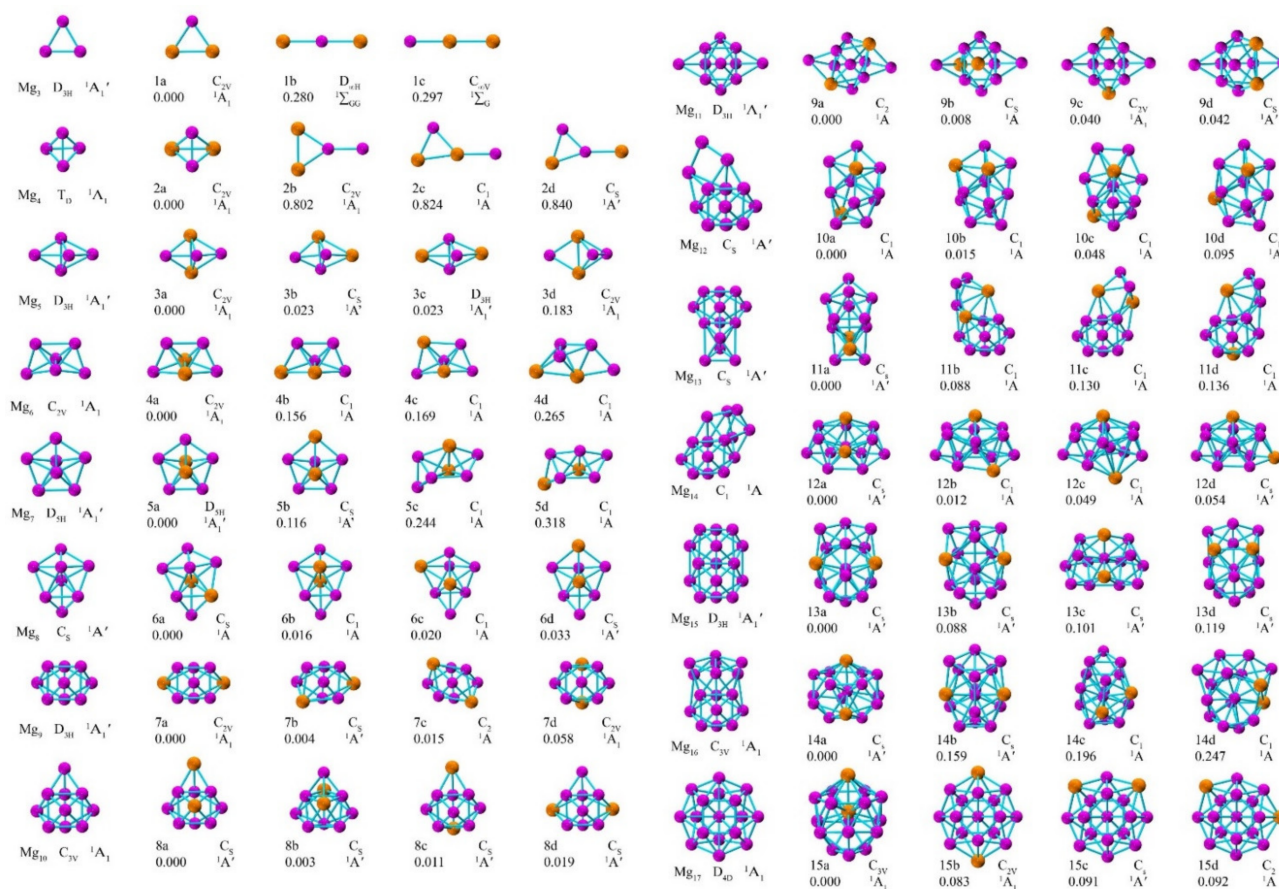

Figure 1. Optimized geometrical structures of lowest and low-lying isomers of Ca$_2$Mg$_n$ (n = 1–15) clusters and Mg$_{n+2}$ (n = 1–15) clusters along with the point group symmetry, electronic states and relative energy (eV). The pinkish and orange balls are magnesium and calcium atoms, respectively.

First, the lowest energy structures of the Mg$_n$ clusters agree with previous research by Zhang and Li et al. [35,37], which indicates that the present functional and basis sets are reliable. Moreover, the Ca$_2$Mg$_n$ (n = 1–8) clusters possess similar geometric structures compared with the Mg$_{n+2}$ clusters. Second, Ca$_2$Mg possesses a triangular plane structure, and the lowest energy structures of Ca$_2$Mg$_n$ (n = 2–15) clusters maintain a three-dimensional (3D) configuration.

Table 1. Electronic states, symmetries, average binding energies E_b (eV), HOMO–LUMO energy gaps E_g (eV), the second-order difference energy ($\Delta_2 E$) and charges on the Ca atoms of the most stable Ca_2Mg_n (n = 1–15) clusters.

Clusters	State	Sym.	E_b (eV)	$\Delta_2 E$ (eV)	E_g (eV)	Charge (e)	
						Ca1	Ca2
Ca_2Mg	$^1A_1$	C_{2V}	0.20	-	1.91	0.11	0.11
Ca_2Mg_2	$^1A_1$	C_{2V}	0.40	0.57	2.01	0.31	0.31
Ca_2Mg_3	$^1A_1$	C_{2V}	0.40	−0.21	1.85	0.37	0.37
Ca_2Mg_4	$^1A_1$	C_{2V}	0.44	−0.25	1.71	0.41	0.41
Ca_2Mg_5	$^1A_1{}'$	D_{5H}	0.50	0.33	1.39	0.53	0.53
Ca_2Mg_6	^1A	D_{5H}	0.51	−0.37	1.51	0.37	0.37
Ca_2Mg_7	$^1A_1$	C_{2V}	0.56	−0.19	1.31	0.68	0.68
Ca_2Mg_8	$^1A'$	C_S	0.61	0.66	1.77	0.84	0.94
Ca_2Mg_9	^1A	C_2	0.60	−0.20	1.77	0.71	0.71
Ca_2Mg_{10}	^1A	C_1	0.60	−0.19	1.16	0.86	0.71
Ca_2Mg_{11}	^1A	C_S	0.62	0.14	1.13	0.87	0.71
Ca_2Mg_{12}	$^1A'$	C_S	0.63	−0.42	1.12	0.85	0.85
Ca_2Mg_{13}	$^1A'$	C_S	0.66	0.06	1.19	0.86	0.86
Ca_2Mg_{14}	$^1A'$	C_S	0.69	−0.06	0.93	1.06	1.06
Ca_2Mg_{15}	$^1A_1$	C_{3V}	0.71	-	1.41	−0.18	0.85

Specifically, Ca_2Mg_n (n = 2–6) clusters can be obtained by adding one Mg atom to the Ca_2Mg_{n-1} clusters, and Ca_2Mg_n (n = 7–9) clusters can be generated from the substitution of Mg_{n+2} clusters by two Ca atoms, respectively. Interestingly, the lowest energy structure of the Ca_2Mg_8 cluster possesses the same geometrical form as those of X_2Mg_8 (X = Be, Sr and Ba) clusters. Finally, from 2 to 14, the doped two Ca atoms prefer to locate outside the host Mg_{n+2} cluster. At n = 15, one Ca atom starts to move from the surface into the internal of the caged skeleton.

3.2. Relative Stability

To determine the relative stabilities of Ca_2Mg_n and Mg_{n+2} (n = 1–15) clusters, the average binding energy (E_b) and second-order difference of energy $\Delta_2 E$ are calculated as follows:

$$
\begin{aligned}
E_b(Ca_2Mg_n) &= \frac{nE(Mg) + 2E(Ca) - E(Ca_2Mg_n)}{n+2} \\
E_b(Mg_n) &= \frac{nE(Mg) - E(Mg_n)}{n} \\
\Delta_2(Ca_2Mg_n) &= E(Ca_2Mg_{n-1}) + E(Ca_2Mg_{n+1}) - 2E(Ca_2Mg_n) \\
\Delta_2 E(Mg_n) &= E(Mg_{n-1}) + E(Mg_{n+1}) - 2E(Mg_n)
\end{aligned}
\tag{1}
$$

E denotes the total energy of the corresponding clusters or atoms. The calculated results are plotted in Table 1 and Figure 2A,B. The following information can be concluded: (1) The values of $E_b(Mg_{n+2})$ clusters are lower than those of $E_b(Ca_2Mg_n)$ clusters, indicating that the doped Ca atom can improve the stability of pure magnesium clusters. (2) With an increase of Mg atoms, the values of E_b (Mg_{n+2} and Ca_2Mg_n) monotonically increase, which indicates an enhanced effect on the stabilities for Ca_2Mg_n and Mg_{n+2} (n = 1–15) clusters. (3) $\Delta_2 E$ values show a certain degree of oscillation, and there exist four visible peaks in the curves at n = 2, 5, 8, 11 and 13, implying that the $Ca_2Mg_{2,5,8,11,13}$ and $Mg_{4,7,10,13,15}$ clusters possess higher relative stability. Most interestingly, the Ca_2Mg_8 cluster with 20 valence electrons possesses an notably high $\Delta_2 E$ value (0.66 eV), which indicates superior relative stability.
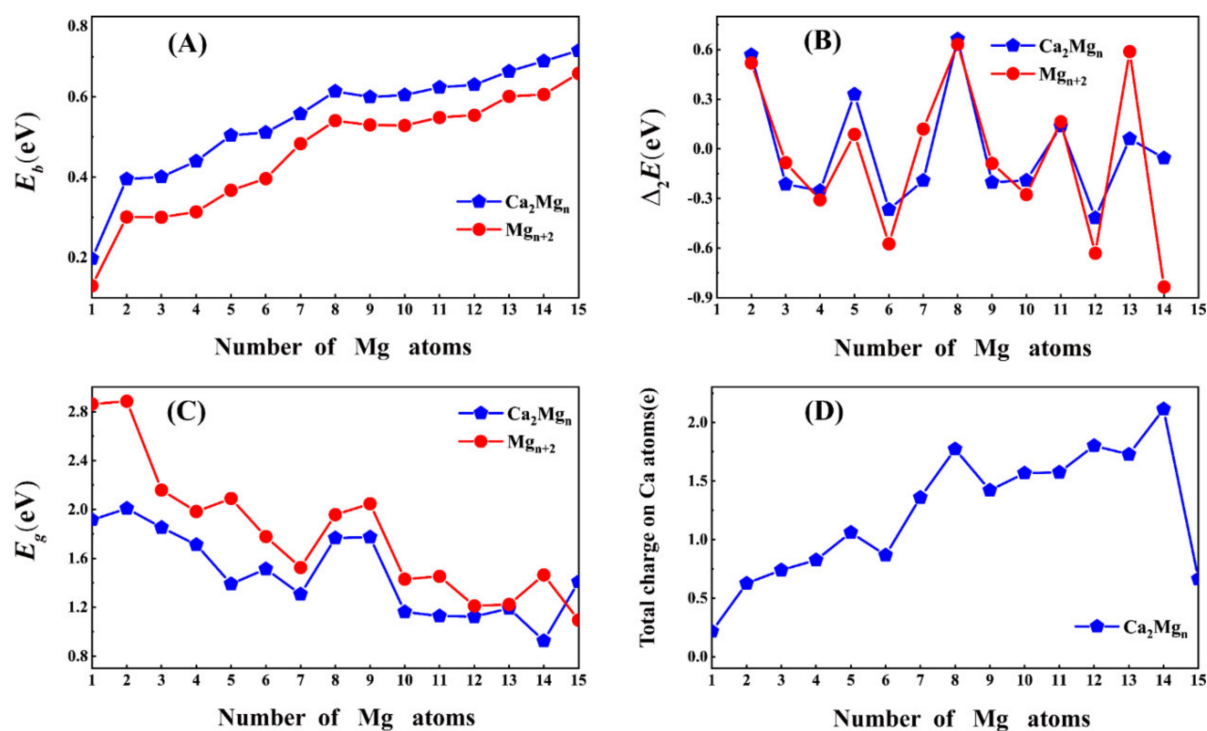
Figure 2. (**A**) E_b, (**B**) $\Delta_2 E$, (**C**) E_g and (**D**) the total charges on Ca atoms in the ground state of Ca$_2$Mg$_n$ (n = 1–15) clusters.

The HOMO–LUMO energy gap (E_g) is the other powerful tool to study the relative stabilities. Generally speaking, large values indicate stronger stability. In the present section, the HOMO–LUMO energy gaps are presented in Table 2 and Figure 2C. First, values of E_g(Mg$_{n+2}$) are larger than those of E_g(Ca$_2$Mg$_n$) clusters, indicating that Ca$_2$Mg$_n$ clusters are more stable, which is in reasonable agreement with previous research on averaged binding energies.

Table 2. The HOMO and LUMO energy of Ca$_2$Mg$_n$ and Mg$_{n+2}$ (n = 1–15).

Clusters	HOMO (eV)	LUMO (eV)	Clusters	HOMO (eV)	LUMO (eV)
Ca$_2$Mg	−3.834	−1.920	Mg$_3$	−4.799	−1.937
Ca$_2$Mg$_2$	−3.981	−1.973	Mg$_4$	−4.961	−2.076
Ca$_2$Mg$_3$	−3.831	−1.979	Mg$_5$	−4.258	−2.099
Ca$_2$Mg$_4$	−3.860	−2.148	Mg$_6$	−4.294	−2.311
Ca$_2$Mg$_5$	−3.531	−2.140	Mg$_7$	−4.436	−2.347
Ca$_2$Mg$_6$	−3.897	−2.384	Mg$_8$	−4.284	−2.507
Ca$_2$Mg$_7$	−3.917	−2.611	Mg$_9$	−4.393	−2.868
Ca$_2$Mg$_8$	−3.954	−2.188	Mg$_{10}$	−4.306	−2.350
Ca$_2$Mg$_9$	−4.048	−2.275	Mg$_{11}$	−4.385	−2.338
Ca$_2$Mg$_{10}$	−3.750	−2.588	Mg$_{12}$	−4.012	−2.583
Ca$_2$Mg$_{11}$	−3.671	−2.543	Mg$_{13}$	−4.105	−2.652
Ca$_2$Mg$_{12}$	−3.746	−2.623	Mg$_{14}$	−4.092	−2.881
Ca$_2$Mg$_{13}$	−3.730	−2.539	Mg$_{15}$	−3.973	−2.750
Ca$_2$Mg$_{14}$	−3.518	−2.592	Mg$_{16}$	−3.985	−2.521
Ca$_2$Mg$_{15}$	−3.965	−2.558	Mg$_{17}$	−3.917	−2.823

Second, Ca$_2$Mg$_{2,6,8,9,15}$ clusters with local maxima of E_{gap} suggests that those clusters are more stable than their neighbors. In summary, combining the conclusions of E_b, $\Delta_2 E$ and E_g values, the Ca$_2$Mg$_8$ cluster corresponds to the magic numbers and exhibits robust stability.

3.3. Charge Transfer

In this section, the charge-transfer information is analyzed by natural population analysis (NPA) in Table 1 and Figure 2D. Clearly, the doped Ca atoms possess positive charges in doped systems, meaning the charges transfer from calcium to magnesium atoms.

Thus, the role of magnesium atoms is as charge acceptors, and Ca atoms are the charge donors. This is expected as Ca (1.00) has a smaller electronegativity compared with that of Mg (1.31) [57]. Second, the transferred charges increase with increasing cluster size. However, the value falls sharply at $n = 15$, and this situation may be the result of the position of Ca atom in the caged skeleton. In addition, the transfer charges in the range of $n = 5$–14 are all greater than 1.0 eV except for Ca_2Mg_6.

3.4. Infrared (IR) and Raman Spectra

In order to facilitate the characterization of spectra, we computationally simulated the infrared (IR) and Raman spectra of the lowest energy structures of Ca_2Mg_8 cluster. The simulated spectra with atomic labels are shown in Figure 3. The results found the highest intense IR frequency was located at 197.74 cm^{-1} with 4Mg-7Mg-10Mg bond tensile vibration; however, two Ca atoms were almost silent. The second and third strongest peaks can be found at 129.62 and 218.78 cm^{-1}. For Raman spectra, the strongest peak at 181.51 cm^{-1} corresponds to the breathing vibration of all atoms. The second- and third-strongest Raman frequencies at 138.28 and 129.62 cm^{-1} correspond to the swing vibration of all atoms. In addition, IR and Raman spectra revealed that the strongest spectral frequencies are displayed in the range of 100–200 cm^{-1}.
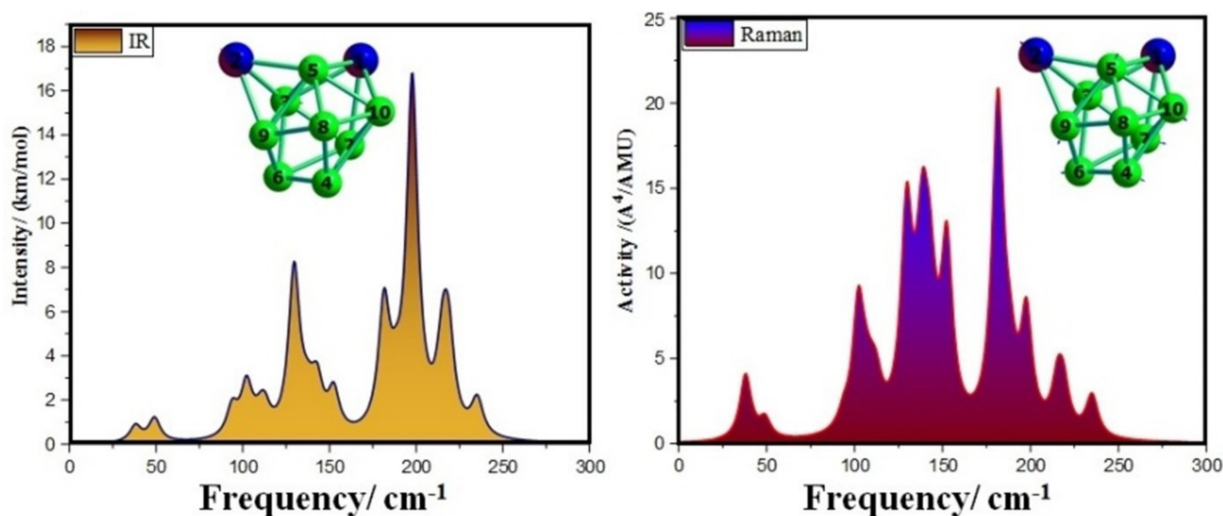

Figure 3. The Infrared and Raman spectra of the most stable cluster of the Ca_2Mg_8 cluster.

3.5. The Density of States

To understand the nature of the chemical bonding, the total density of states (TDOS) and partial density of states (PDOS) of the lowest energy structures of Ca_2Mg_n ($n = 1$–15) are displayed in Figure 4. The TDOS is represented by the khaki shade; PDOS of Ca-*s*, Ca-*p*, Mg-*s* and Mg-*p* AOs (atomic orbitals) are represented by the red and blue solid lines as well as magenta and green dotted lines, respectively. We found that the contribution to TDOS mainly comes from the PDOS of Ca-*s*, Mg-*s* and Mg-*p* AOs in the region of occupied orbitals.
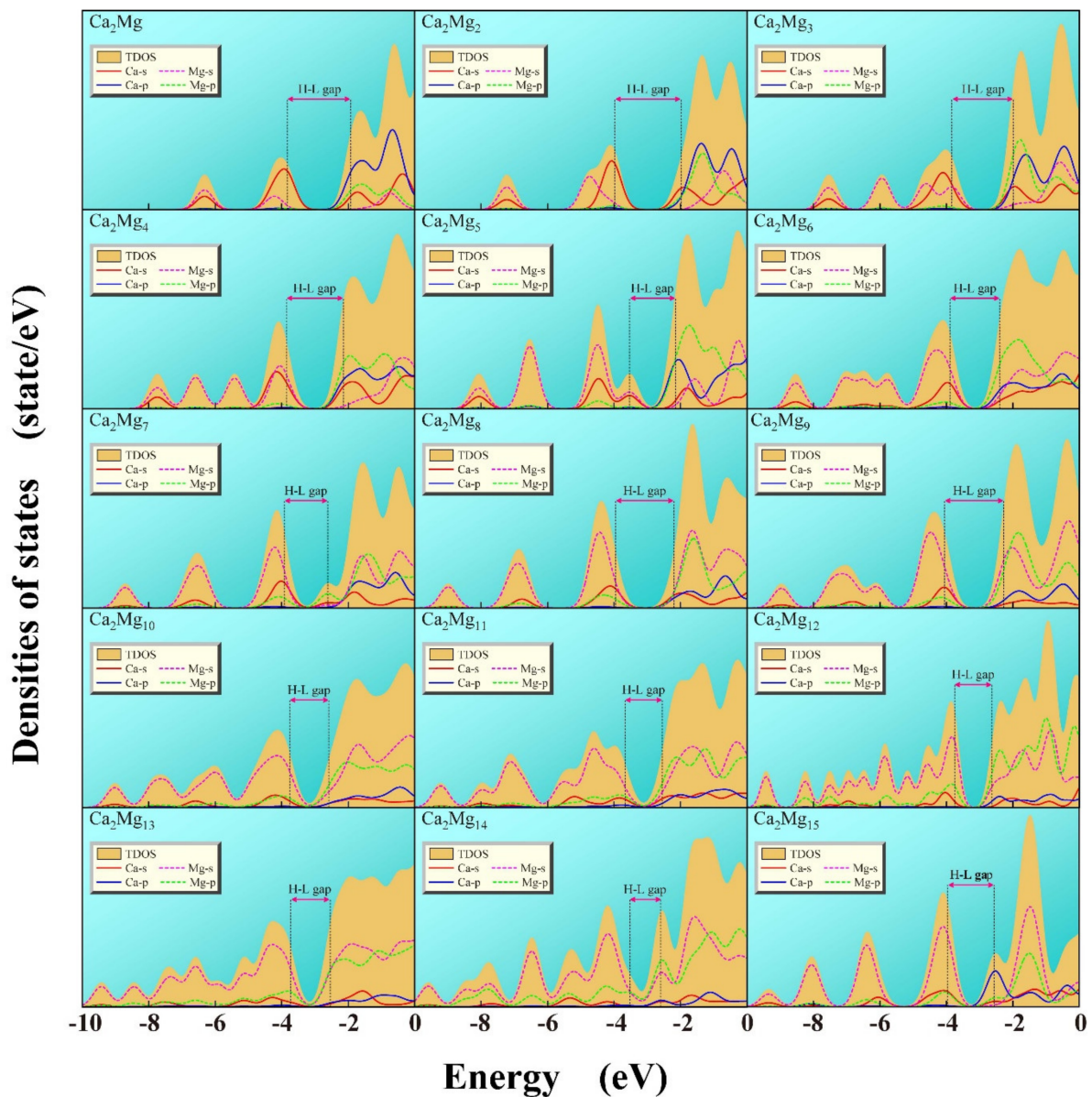
Figure 4. The calculated total densities of states (TDOS) and partial densities of states (PDOS) of Ca_2Mg_n (n = 1–15) clusters.

This indicates that *sp* hybridization has occurred in Ca-Mg atoms and Mg-Mg atoms. In fact, the *sp* hybridization of Mg-Mg promotes the formation of Mg_n frames in Ca_2Mg_n clusters. The *sp* hybridization of Ca-Mg can promote the interaction between the two doped calcium atoms and magnesium frames of Ca_2Mg_n clusters, which is also the main reason why the stability of Ca_2Mg_n is higher than that of their corresponding pure magnesium clusters.

3.6. Bonding Characters

Based on the above analyses, a pagoda-like Ca_2Mg_8 structure possesses superior stability. To illustrate the source of higher stability, the bonding nature, such as the MOs (molecular orbitals) and multi-center bonds, are discussed for the lowest energy structure of Ca_2Mg_8 cluster. The molecular energy levels and corresponding orbitals are presented in Figure 5. First, calcium and magnesium atoms are composed of the same valence configuration of s^2, and Ca_2Mg_8 with 20 valence electrons meets the requirement of the Jellium model in terms of the valence electron number.
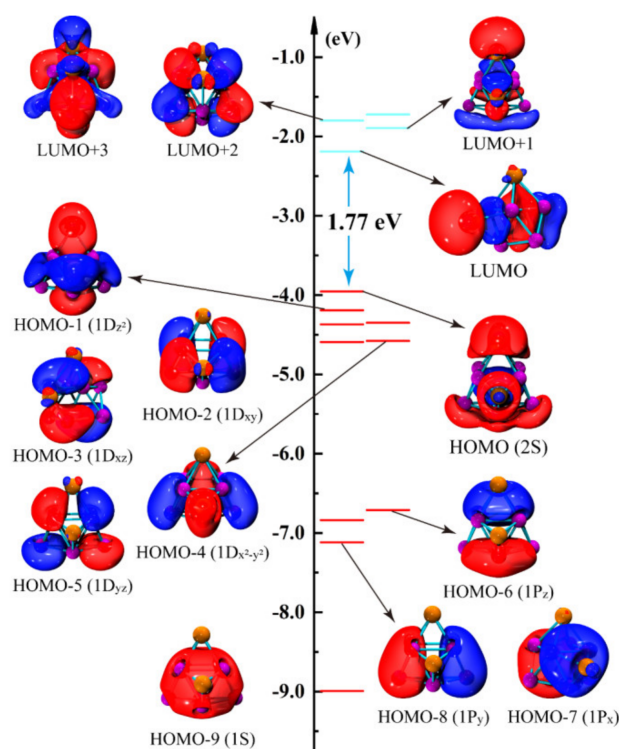
Figure 5. Molecular orbitals and the corresponding energy levels of the Ca_2Mg_8 cluster. The HOMO–LUMO gap is indicated (in azure).

Moreover, the shell structures consist of one 1S orbital, three 1P orbital, five 1D orbitals and one 2S orbital, all of which are occupied by the paired electrons. The energy of 1S, 1P, 1D and 2S states are arranged in order from low to high without energy levels overlapping, and the energy levels are also relatively concentrated. In addition, all the splitting energy levels of 1D orbital are lower in energy than the 2S orbital. As a result, Ca_2Mg_8 cluster is a closed shell $1S^2 1P^6 1D^{10} 2S^2$ filled with 20 valence electrons.

In addition, the contributions of molecular orbital for Ca_2Mg_8 cluster were probed utilizing Multiwfn 3.8 program. The HOMO corresponding to 2S state involves Ca-*s* (30.98%), Mg-*s* (19.53%) and Mg-*p* (44.86%). The HOMO-*m* (*m* = 1–5) exhibit 1D state, in which HOMO-1 and HOMO-4 are mainly composed of Ca-*s* (10.62%, 26.60%), Mg-*s* (41.87%, 16.99% for) and Mg-*p* (43.70%, 53.33%), respectively, and the remaining 1D state orbital is mainly contributed to by Mg atoms. The compositions of HOMO-6, 7, 8 corresponding to three 1P orbitals comes mainly from the Mg-*s* and *p* AOs as well as to a small extent from the Ca-*s* and *p* AOs. In the case of HOMO-9 (1S), Mg atoms provide more than 90% of the orbital contribution. Hence, the *sp* hybridization between the Ca and Mg atoms could promote the interaction between the doped-Ca and host-Mg atoms and form stronger Ca-Mg bonds.

To further elucidate the bonding patterns of the Ca_2Mg_8 cluster, adaptive natural density partitioning (AdNDP) is included, representing the bonding of a molecule in terms of *n*-center two-electron (*nc*-2e) bonds. Notably, 1c-2e and 2c-2e bonds mean a localized character; the *nc*-2e bond ($n \geq 3$) belongs to the delocalized character. For the Ca_2Mg_8 cluster, ten delocalized bonds with different occupation number (ON) are shown in Figure 6, which corresponds to three delocalized 3c-2e σ-bonds, two delocalized 4c-2e σ-bonds, two delocalized 5c-2e π-bonds, two delocalized 7c-2e π-bonds and one delocalized 9c-2e π-bond, respectively.
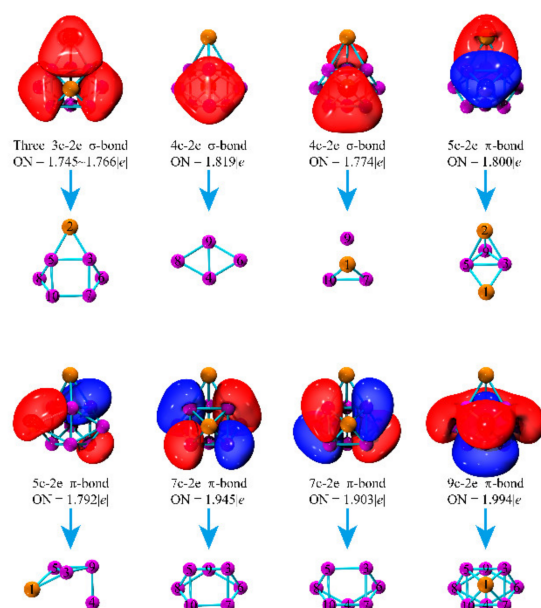
Figure 6. AdNDP chemical bonds and the corresponding structural units for the Ca_2Mg_8 cluster. (ON denotes the occupation number).

Three 3c-2e σ-bonds with an ON of 1.745–1.766 |e| are formed by two opposite trigonal 5Mg-8Mg-10Mg and 3Mg-6Mg-7Mg units and one 2Ca-5Mg-3Mg unit. Two 4c-2e σ-bonds are accountable for the bonding between the quadrangle 4Mg-6Mg-8Mg-9Mg units (ON = 1.89 |e|) and pyramid 1Ca-7Mg-9Mg-10Mg units (ON = 1.774 |e|), respectively. There are two 5c-2e π-type bonds with ON = 1.80 and 1.792 |e|, derived from two Ca-Mg units of 1Ca-2Ca-3Mg-5Mg-9Mg and 1Ca-3Mg-4Mg-5Mg-9Mg units, respectively. Two 7c-2e ON = 1.945, 1.903 |e| (two symmetric units) and one 9c-2e ON = 1.994 |e| exhibit π-type bonding character. In addition, to deeply understand the nature of bonding, the Wiberg bond orders are calculated and listed in Table 3. The results indicate that the strong Ca-Mg bonds are greater than Ca-Ca and most Mg-Mg bonds.

Table 3. The Wiberg bond orders of the Ca_2Mg_8 cluster.

Atoms	Ca-1	Ca-2	Mg-3	Mg-4	Mg-5	Mg-6	Mg-7	Mg-8	Mg-9
Ca-2	0.130								
Mg-3	0.383	0.462							
Mg-4	0.151	0.143	0.233						
Mg-5	0.383	0.462	0.524	0.233					
Mg-6	0.139	0.131	0.517	0.529	0.228				
Mg-7	0.398	0.149	0.528	0.439	0.237	0.523			
Mg-8	0.139	0.131	0.228	0.529	0.517	0.182	0.199		
Mg-9	0.179	0.410	0.465	0.458	0.465	0.487	0.231	0.487	
Mg-10	0.398	0.149	0.237	0.439	0.528	0.199	0.523	0.523	0.231

4. Conclusions

In summary, a detailed investigation of the structures and electronic properties of Ca_2Mg_n (n = 1–15) was performed using the CALYPSO searching method and DFT calculations. Structural searching found that two Ca atoms prefer to occupy the external position of magnesium-doped systems at n = 2–14 and that one Ca atom tends to move from the surface into the internal of the caged skeleton at n = 15. The size-dependent binding energies, second-order difference of energies, and HOMO–LUMO gaps found a pagoda-like Ca_2Mg_8 as a magic cluster that possessed higher stability.

Upon charge transfer analysis, charges transferred from calcium to magnesium atoms. The simulated IR and Raman spectra of the magic cluster revealed that the strongest spectral frequencies were displayed in the range of 100~200 cm^{-1}. In addition, the high stability of Ca$_2$Mg$_8$ with a 20 valence electron cluster possessed a closed-shell electron configuration of 1S^{2}1P^{6}1D^{10}2S^2 in terms of the Jellium model. Last, the *sp* hybridization of Ca-Mg and Mg-Mg bonds was confirmed by the molecular orbitals and AdNDP, which contribute to the high stability of the Ca$_2$Mg$_8$ cluster.

Supplementary Materials: The following supporting information can be downloaded at: https://www.mdpi.com/article/10.3390/nano12101654/s1, Table S1: Cartesian coordinates for the lowest energy structures of Ca$_2$Mg$_n$ (*n* = 1–15) clusters.

Author Contributions: C.L.: investigation, writing—original draft and funding acquisition. Y.C.: investigation and writing—review and editing. H.T. and B.R.: investigation and software. Q.L. and Y.L.: writing—review and editing and supervision. H.Y.: conceptualization and supervision. All authors have read and agreed to the published version of the manuscript.

Institutional Review Board Statement: Not applicable.

Informed Consent Statement: Not applicable.

Data Availability Statement: The data are included in the main text.

Conflicts of Interest: The authors declare no conflict of interest.

References

1. Nanan, M.E.; Bierwagen, G.P. Mg-Rich coatings: A new paradigm for Cr-free corrosion protection of Al arrospece alloy. *JCT Res.* **2014**, *1*, 69–80.
2. Yoo, J.; Aksimentiev, A. Improved parametrization of Li$^+$, Na$^+$, K$^+$ and Mg^{2+} ions for all-atom molecular dynamics simulations of nucleic acid systems. *J. Phys. Chem. Lett.* **2012**, *3*, 45–50. [CrossRef]
3. Pollock, T.M. Weight loss with magnesium alloys. *Science* **2010**, *328*, 986–987. [CrossRef] [PubMed]
4. Kim, S.H.; You, B.S.; Yim, C.D. Texture and microstructure changes in asymmetrically hot rolled Az$_{31}$ magnesium alloy sheets. *Mater. Lett.* **2005**, *59*, 3876–3880. [CrossRef]
5. Diederich, T.; Doppner, T.; Braune, J.; Tiggesbaumker, J.; Meiwes-Broer, K.H. Electron delocalization in magnesium clusters grown in superclod helium drolpets. *Phys. Rev. Lett.* **2001**, *86*, 4807–4810. [CrossRef]
6. Thomas, O.C.; Zheng, W.J.; Xu, S.J.; Bowen, K.H. Onset of metallic behavior in magnesium clusters. *Phys. Rev. Lett.* **2002**, *89*, 213403. [CrossRef]
7. Li, P.; Xie, W.; Tang, K.T. The van der Waals potential of the magnesium dimer. *J. Chem. Phys.* **2010**, *133*, 084308. [CrossRef]
8. Janecek, S.; Krotscheck, E.; Liebrecht, M.; Wahl, R. Structure of Mg$_n$ and Mg$_n^+$ clusters up to n = 30. *Eur. Phys. J. D-At. Mol. Opt. Plasma Phys.* **2011**, *63*, 377–390. [CrossRef]
9. Kaplan, I.G.; Diaz, C.C. Comparative study of the electron affinities of beryllium and magnesium dimmers and trimers. *Int. J. Quantum Chem.* **2005**, *104*, 468–474. [CrossRef]
10. Gong, X.G.; Zheng, Q.Q.; He, Y.Z. Electronic structures of magnesium clusters. *Phys. Lett. A* **1993**, *181*, 459–464. [CrossRef]
11. Akola, J.; Rytkonen, K.; Manninen, M. Metallic evolution of small magnesium clusters. *Eur. Phys. J. D* **2001**, *16*, 21–24. [CrossRef]
12. Jellinek, J.; Acioli, P.H. Magnesium Clusters: Structural and Electronic Properties and the Size-Induced Nonmetal-to-Metal Transition. *J. Phys. Chem. A* **2002**, *106*, 10919–10925. [CrossRef]
13. Acioli, P.H.; Jellinek, J. Electron binding energies of anionic magnesium clusters and the nonmetal-to-metal transition. *Phys. Rev. Lett.* **2002**, *89*, 213402. [CrossRef]
14. Lyalin, A.; Solov'yov, I.A.; Solov'yov, A.V.; Greiner, W. Evolution of the electronic and ionic structure of Mg clusters with increase in cluster size. *Phys. Rev. A* **2003**, *67*, 063203. [CrossRef]
15. Kohn, A.; Weigend, F.; Ahlrichs, R. Theoretical study on clusters of magnesium. *Phys. Chem. Chem. Phys.* **2001**, *23*, 711–719. [CrossRef]
16. Herdari, I.; Ghazi, S.M.; Goedecker, S.; Kanhere, D.G. Growth and structural properties of Mg$_n$ (n = 10–56) clusters: Density functional theory study. *J. Phys. Chem. A* **2011**, *115*, 12307–12314. [CrossRef]

17. Xia, X.X.; Kuang, X.Y.; Lu, C.; Jin, Y.Y.; Xing, X.D.; Merino, G. Deciphering the structural evolution and electronic properties of magnesium clusters: An aromatic homonuclear metal. *J. Phys. Chem. A* **2016**, *120*, 7947–7954. [CrossRef]

18. Duanmu, K.; Roberto-Neto, O.; Machado, F.B.C.; Hansen, J.A.; Shen, J.; Piecuch, P.; Truhlar, D.G. Geometries, binding energies, ionization potentials, and electron affinities of metal clusters: $Mg_n^{0,\pm1}$, n = 1–7. *J. Phys. Chem. C* **2016**, *120*, 13275. [CrossRef]

19. Duanmu, K.; Friedrich, J.; Truhlar, D.G. Thermodynamics of metal nonparties: Energies and enthalpies of formation of magnesium clusters and nanoparticles as large as 1.3 nm. *J. Phys. Chem. C* **2016**, *120*, 26110. [CrossRef]

20. Kong, F.J.; Hu, Y.F. Density functional theory study of small X-doped Mg_n (X = Fe, Co, and Ni, *n* = 1–9) bimetallic clusters: Equilibrium structures, stabilities, electronic and magnetic properties. *J. Mol. Model.* **2014**, *20*, 2087. [CrossRef]

21. Ge, G.X.; Han, Y.; Wan, J.G.; Zhao, J.J.; Wang, G.H. First-principles prediction of magnetic superatoms in 4*d*-transition-metal-doped magnesium clusters. *J. Chem. Phys.* **2013**, *139*, 174309. [CrossRef] [PubMed]

22. Li, Z.; Zhao, Z.; Zhou, Z.H.; Wang, H.B.; Li, S.L. First-principles calculations on small Mg_nZn and $Mg_{n-1}Zn_2$ clusters: Structures, stabilities, and electronic properties. *Mater. Chem. Phys.* **2017**, *199*, 585–590. [CrossRef]

23. Xing, X.D.; Wang, J.J.; Kuang, X.Y.; Xia, X.X.; Lu, C.; Maroulis, G. Probing the low-energy structures of aluminum-magnesium alloy clusters: A detailed study. *Phys. Chem. Chem. Phys.* **2016**, *18*, 26177–26183. [CrossRef] [PubMed]

24. Trivedi, R.; Bandyopadhyay, D. Study of absorption and dissociation pathway of H_2 molecule on Mg_nRh (*n* = 1–10) clusters: A first principle investigation. *Int. J. Hydrogen Energy* **2016**, *41*, 20113–20121. [CrossRef]

25. Afshar, M.; Chegeni, M.H. Spin and orbital magnesium in XMg_8 (X = Sc-Ni): A relativistic density functional theory study. *Mol. Phys.* **2016**, *114*, 3620–3628. [CrossRef]

26. Medel, V.M.; Ulises, J.; Khanna, S.N.; Chauhan, V.; Sen, P.; Castleman, A.W. Hund's rule in superatoms with transition metal impurities. *Proc. Natl. Acad. Sci. USA* **2011**, *108*, 10062–10066. [CrossRef]

27. Zhu, B.C.; Zhang, S.; Zeng, L. The effect of silicon doping on the geometrical structures, stability, and electronic and spectral properties of magnesium clusters: DFT study of $SiMg_n$ (*n* = 1–12) clusters. *Int. J. Quantum Chem.* **2020**, *120*, e26143. [CrossRef]

28. Medel, V.M.; Reber, R.C.; Reveles, J.U.; Khanna, S.N. Metallic and molecular orbital concepts in XMg_8 clusters, X = Be-F. *J. Chem. Phys.* **2012**, *136*, 134311. [CrossRef]

29. Zeng, L.; Liang, M.K.; Wei, X.F.; Guo, J.; Zhu, B.C. New potential stable structures of XMg_n (X = Ge, C, Sn; *n* = 1–12) clusters: XMg_8 with high stability. *J. Phys. Condens. Matter* **2021**, *33*, 065302. [CrossRef]

30. Trivedi, R.; Bandyopadhyay, D. Hydrogen storage in small size Mg_nCo clusters: A density functional study. *Int. J. Hydrogen Energy* **2015**, *40*, 12727–12735. [CrossRef]

31. Lu, C.; Ma, Y.L.; Li, F.; Zhu, H.; Zeng, X.Q.; Ding, W.J.; Deng, T.; Wu, J.B.; Zhou, J.X. Visualization of fast "hydrogen pump" in core–shell nanostructure Mg@Pt through hydrogen-stabilized Mg_3Pt. *J. Mater. Chem. A* **2019**, *7*, 14629–14637. [CrossRef]

32. Zeng, L.; Wei, X.F.; Liang, M.K.; Zhao, J.; Zhu, B.C. Probing on the Stable Structure of Silicon-Doped Charged Magnesium Nanomaterial Sensor: $SiMg_n^{\pm1}$ (n = 2−12) Clusters DFT Study. *Front. Mater.* **2020**, *7*, 221. [CrossRef]

33. Zeng, L.; Liang, M.K.; Wei, X.F.; Guo, J.; Zhang, S.; Bi, J.; Dai, W.; Zhu, B.C. Probing the structural evolution, electronic and spectral properties of beryllium doped magnesium and their ions clusters. *New J. Chem.* **2020**, *44*, 16929–16940. [CrossRef]

34. Zhao, Y.R.; Xu, Y.Q.; Chen, P.; Yuan, Y.Q.; Qian, Y.; Li, Q. Structural and electronic properties of medium-sized beryllium doped magnesium $BeMg_n$ clusters and their anions. *Results Phys.* **2021**, *26*, 104341. [CrossRef]

35. Zhang, F.G.; Zhang, H.R.; Xin, W.; Chen, P.; Hu, Y.F.; Zhang, X.Y.; Zhao, Y.R. Probing the structural evolution and electronic properties of divalent metal Be_2Mg_n clusters from small to medium-size. *Sci. Rep.* **2020**, *10*, 6052. [CrossRef]

36. Li, Q.Y.; Xi, S.G.; Hu, Y.F.; Yuan, Y.Q.; Zhao, Y.R.; Li, M.C.; Yuan, J.J.; Yang, Y.J. Probing the structural and electronic properties of neutral and anionic strontium-doped magnesium clusters. *Comput. Mater. Sci.* **2021**, *197*, 110605. [CrossRef]

37. Li, Q.Y.; Hu, Y.F.; Xi, S.G.; Li, Y.Y.; Yang, H.; Yuan, Y.Q.; Yang, J.; Li, M.C. Structural and electronic properties of neutral and anionic magnesium clusters doped with two barium atoms. *J. Mol. Liq.* **2021**, *343*, 117622. [CrossRef]

38. Li, C.G.; Cui, Y.Q.; Tian, H.; Shao, Q.Q.; Zhang, J.; Ren, B.Z.; Yuan, Y.Q. Systematic investigation of geometric structures and electronic properties of lithium doped magnesium clusters. *Comput. Mater. Sci.* **2021**, *200*, 110800. [CrossRef]

39. Wang, Y.C.; Lv, J.; Zhu, L.; Ma, Y.M. Crystal structure prediction via particle swarm optimization. *Phys. Rev. B Condens. Matter Mater. Phys.* **2010**, *82*, 094116. [CrossRef]

40. Wang, Y.C.; Lv, J.; Zhu, L.; Ma, Y.M. CALYPSO: A method for crystal structure prediction. *Comput. Phys. Commun.* **2012**, *183*, 2063–2070. [CrossRef]

41. Lv, J.; Wang, Y.C.; Zhu, L.; Ma, Y.M. Particle swarm structure prediction on clusters. *J. Chem. Phys.* **2012**, *137*, 084104. [CrossRef]

42. Chen, B.L.; Sun, W.G.; Kuang, X.Y.; Lu, C.; Xia, X.X.; Shi, H.X.; Maroulis, G. Structural Stability and Evolution of Medium-Sized Tantalum-Doped Boron Clusters: A Half-Sandwich-Structured TaB_{12}^- Cluster. *Inorg. Chem.* **2018**, *57*, 343–350. [CrossRef]

43. Li, C.G.; Li, H.J.; Cui, Y.Q.; Tian, H.; Shao, Q.Q.; Zhang, J.; Zhao, G.; Ren, B.Z.; Hu, Y.F. A density functional investigation on the structures, electronic, spectral and fluxional properties of VB_{20}^- cluster. *J. Mol. Liq.* **2021**, *339*, 116764. [CrossRef]

44. Zhao, Y.R.; Bai, T.T.; Jia, L.N.; Xin, W.; Hu, Y.H.; Zheng, X.S. Probing the Structural and Electronic Properties of Neutral and Anionic Lanthanum-Doped Silicon Clusters. *J. Phys. Chem. C* **2019**, *123*, 28561–28568. [CrossRef]

45. Lai, L.; Die, D.; Zheng, B.X.; Du, Q. Growth mechanism and electronic and magnetic properties of Ag_nTi alloy clusters. *J. Phys. Chem. Solids* **2021**, *148*, 109757. [CrossRef]

46. Jin, S.Y.; Chen, B.L.; Kuang, X.Y.; Lu, C.; Sun, W.G.; Xia, X.X.; Gutsev, G.L. Structural and Electronic Properties of Medium-Sized Aluminum-Doped Boron Clusters AlB_n and Their Anions. *J. Phys. Chem. C* **2019**, *123*, 6276–6283. [CrossRef]

47. Li, C.G.; Shen, Z.G.; Zhang, J.; Cui, Y.Q.; Li, J.J.; Xue, H.Y.; Li, H.F.; Ren, B.Z.; Hu, Y.F. Analysis of the structures, stabilities and electronic properties of MB_{16}^- (M = V, Cr, Mn, Fe, Co, Ni) clusters and assemblies. *New J. Chem.* **2020**, *44*, 5109–5119. [CrossRef]

48. Lu, C.; Gong, W.G.; Li, Q.; Chen, C.F. Elucidating stress-strain of ZrB_{12} from first-priciples studies. *J. Phys. Chem. Lett.* **2020**, *11*, 9165–9170. [CrossRef] [PubMed]

49. Die, D.; Zheng, B.X.; Yue, J.Y.; Guo, J.J.; Du, Q. The ground-state structure, optical-absorption and photoelectron spectrum of silver clusters. *Phys. E Low-Dimens. Syst. Nanostruct.* **2020**, *117*, 113805. [CrossRef]

50. Li, C.G.; Gao, J.H.; Zhang, J.; Song, W.T.; Liu, S.Q.; Gao, S.Z.; Ren, B.Z.; Hu, Y.F. Structures, stabilities and electronic properties of boron-doped silicon clusters B_3Si_n (n = 1–17) and their anions. *Mol. Phys.* **2019**, *117*, 382. [CrossRef]

51. Krishnan, R. Self-consistent molecular orbital methods. XX. A basis set for correlated wave functions. *J. Chem. Phys.* **1980**, *72*, 650–654. [CrossRef]

52. Tao, J.; Perdew, J.P.; Staroverov, V.N.; Scuseria, G.E. Climbing the Density Functional Ladder: Nonempirical Meta-Generalized Gradient Approximation Designed for Molecules and Solids. *Phys. Rev. Lett.* **2003**, *91*, 146401–146405. [CrossRef]

53. Frisch, M.J.; Trucks, G.W.; Schlegel, H.B.; Scuseria, G.E.; Robb, M.A.; Cheeseman, J.R.; Scalmani, G.; Barone, V.; Petersson, G.A.; Nakatsuji, H.; et al. *Fox, Gaussian 09 Revision D.01*; Gaussian Inc.: Wallingford, CT, USA, 2009.

54. Lu, T.; Chen, F.W. Multiwfn: A multifunctional wavefunction analyzer. *Comput. Phys. Commun.* **2012**, *33*, 580–592. [CrossRef]

55. Ruette, F.; Sanchez, M.; Anez, R.; Bermudez, A.; Sierraalta, A. Diatomic molecule data for parametric methods. I. *J. Mol. Struct. THEOCHEM* **2005**, *729*, 19–37. [CrossRef]

56. Soltani, A.; Boudjahem, A.G.; Bettahar, M. Electronic and magnetic properties of small Rh_nCa (n = 1–9) clusters: A DFT Study. *Int. J. Quantum Chem.* **2016**, *116*, 346–356. [CrossRef]

57. Zhou, G.D.; Duan, L.Y. *Free Movement in the EU: The Case of Great Britain Structural Chemistry Basis*; Peking University Press: Beijing, China, 2002; pp. 1–10.